~~Sandford~~

PERS. COPY OF RUHLIN

ANALYSIS AND MECHANIZATION OF NASA-LANGLEY FLUTTER SAS CONCEPTS

D3-8390-1

THE BOEING COMPANY
WICHITA DIVISION
WICHITA, KANSAS

ABSTRACT

This document discusses results of an active flutter suppression system analysis using a Boeing Supersonic Transport 969-300 configuration. The work was accomplished under NASA-Langley Contract NAS1-9808. Dr. Eliahu Nissim of the NASA-Langley Aeroelasticity Branch, Dynamic Loads Division, developed the two concepts analyzed.

RETRIEVAL REFERENCE WORDS:

REV LTR:

BOEING NO.

PAGE

TABLE OF CONTENTS

1.0 INTRODUCTION AND SUMMARY

This report presents the results of an analytical and mechanization study conducted for two flutter SAS concepts developed by Dr. Eliahu Nissim of the NASA-Langley Aeroelasticity Branch, Dynamic Loads Division. Concept No. 1 utilizes only the wing trailing edge control surface(s). Concept No. 2 utilizes leading and trailing edge control surfaces operating simultaneously. Theoretically, the combined use of leading and trailing edge control surfaces will improve the surface coupling (controllability) with vertical bending and torsional structural modes and decrease the coupling between bending and torsional modes.

The purpose of this study was:

- To determine flutter speed using full scale 969-300 SST equations of motion augmented with flutter SAS concepts No. 1 and No. 2.
- To develop a method of implementing these concepts for wind tunnel testing.

The wing is configured with three leading edge control surfaces (outboard, mid-span and inboard) and three corresponding trailing edge control surfaces. Five combinations of control surfaces and SAS concepts were analyzed during this study. These combinations and corresponding flutter speed improvements are as follows:

- I • 4.5 percent for the outboard trailing edge surface with flutter SAS No. 1.
- II • 11 percent for the leading/trailing (L/T) edge outboard surfaces with SAS No. 2.
- III • 28 percent for the L/T edge mid-span surfaces with SAS No. 2.
- IV • 21 percent for the L/T edge inboard surfaces with SAS No. 2.
- V • Greater than 41 percent for the combined L/T edge inboard and mid-span surfaces with SAS No. 2.

Figure 1 illustrates the flutter problem on an airspeed root locus plot for the combined inboard and mid-span L/T edge surfaces at a constant Mach No. = 0.9. Airspeed was varied by changing altitude while holding Mach number constant. The free airplane encounters instability at 422 KCAS. The airplane augmented with flutter concept No. 2 using both inboard and mid-span surfaces is flutter free for airspeeds up to 595 KCAS (altitude: sea level). Figure 2 presents the third and fourth elastic mode damping ratio as a function of airspeed for the combined surface configuration. Similar plots for each of the other flutter SAS concepts are included in Section 2.0.

NOTES:
1) M = 0.9
2) —— FREE AIRPLANE
3) --- WITH SAS FLUTTER NO. 2
4) FLUTTER SPEED (3RD MODE)
   FREE AIRPLANE: 422 KCAS
   WITH SAS: >595 KCAS

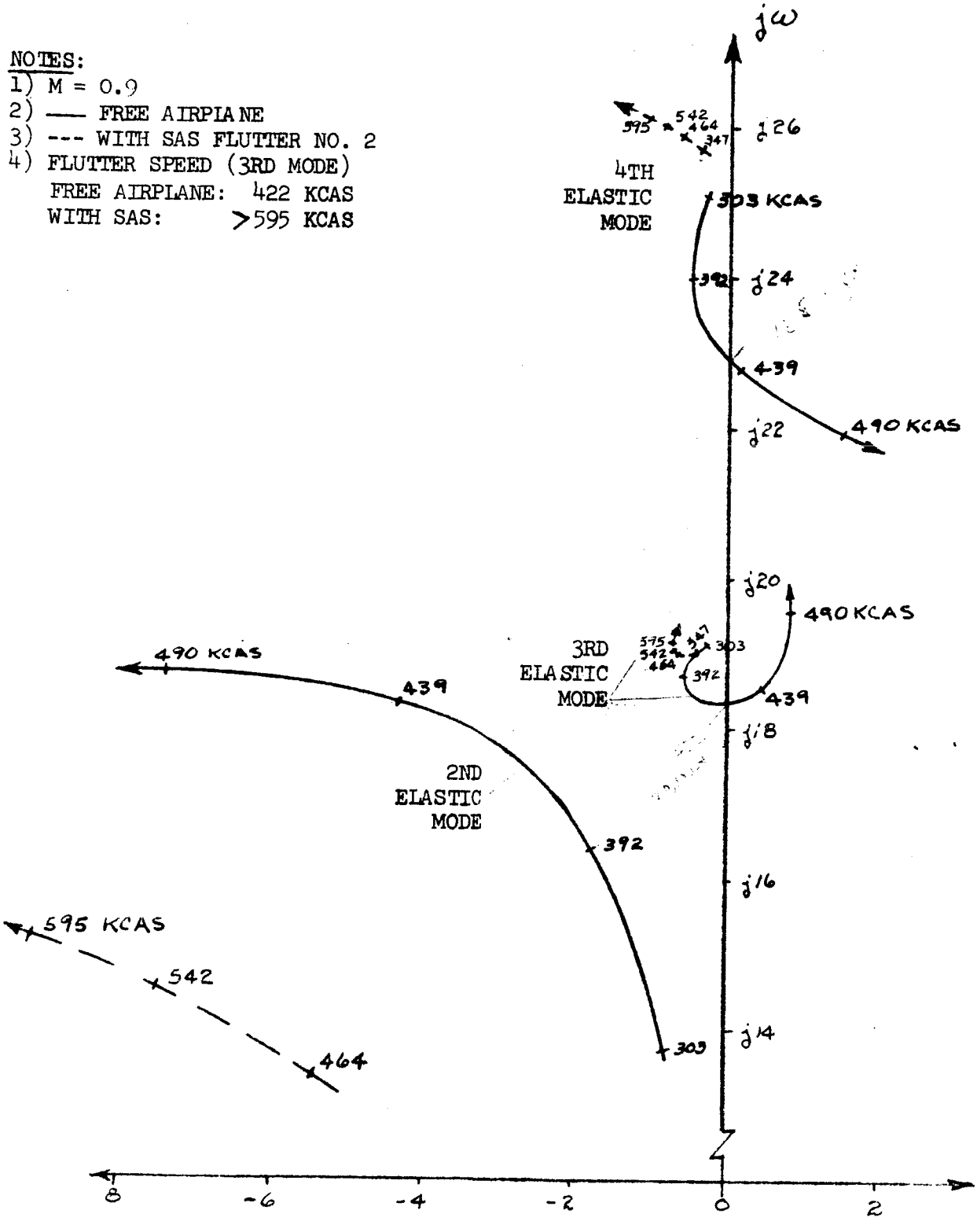

FLUTTER SAS ROOT LOCUS WITH MID-SPAN
AND INBOARD L/T EDGE SURFACES

Figure 1

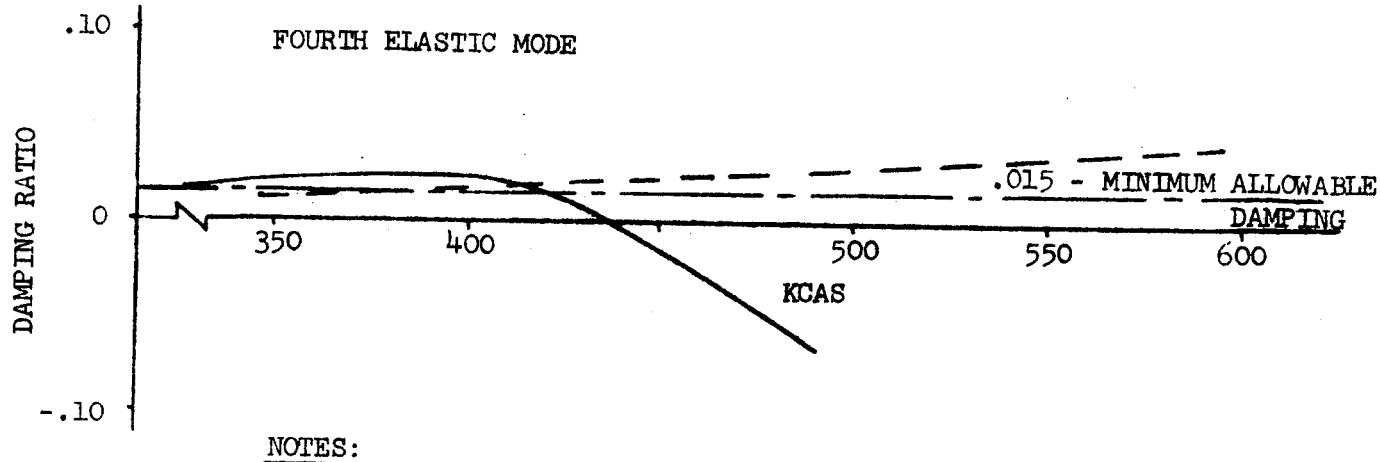

NOTES:
1) ___ FREE AIRPLANE
--- FLUTTER SAS NO. 2 WITH MID-SPAN AND INBOARD L/T SURFACES
2) M = 0.9
3) STRUCTURAL MODE : STABILITY ONLY

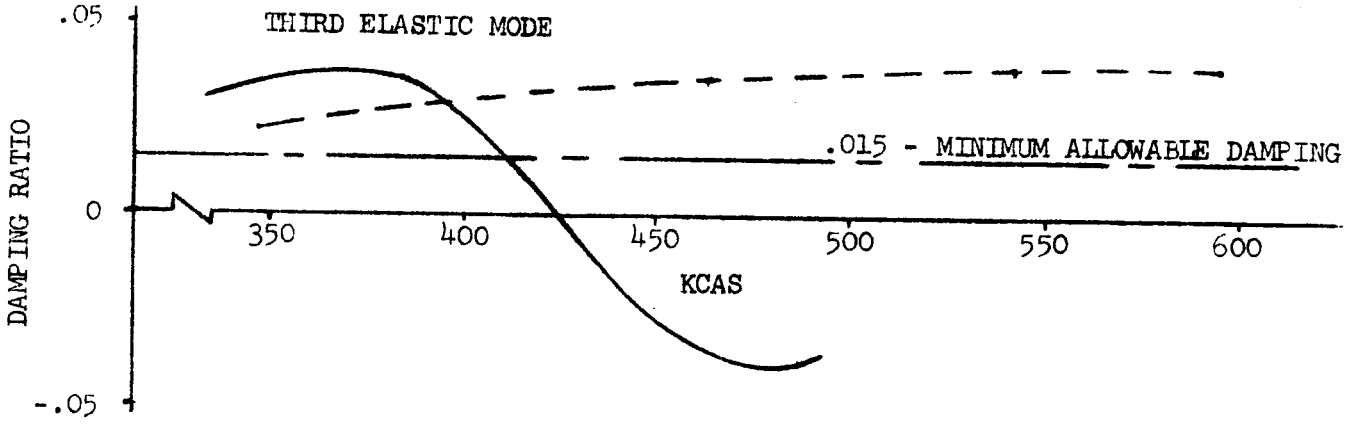

EFFECT OF SAS ON FLUTTER SPEED

Figure 2

All flutter concepts and surface combinations cause a low frequency (phugoid mode) instability at the selected gains. Stability results indicate that phase lead and a decrease in amplitude at this frequency, obtained with a high-pass filter, would stabilize this mode.

Flutter SAS concept No. 1 using an outboard control surface is scheduled to be mechanized and tested on NASA-Langley's 1/17 scale SST wing model.

A block diagram of the system to be mechanized is shown in Figure 3. The primary problem associated with mechanization is that the systems require the rate signal to be divided by frequency. Two methods of mechanizing the flutter augmentation systems were tested on an analog computer to assess the feasibility of measuring instantaneous frequency (period) based on the simple harmonic motion relationship: $\omega^2 = |\text{acceleration}|/|\text{displacement}|$. The other method measures "period" by detecting zero-crossings. Both mechanizations adequately measure the steady-state frequency over the frequency range of primary interest (5 to 25 Hz).

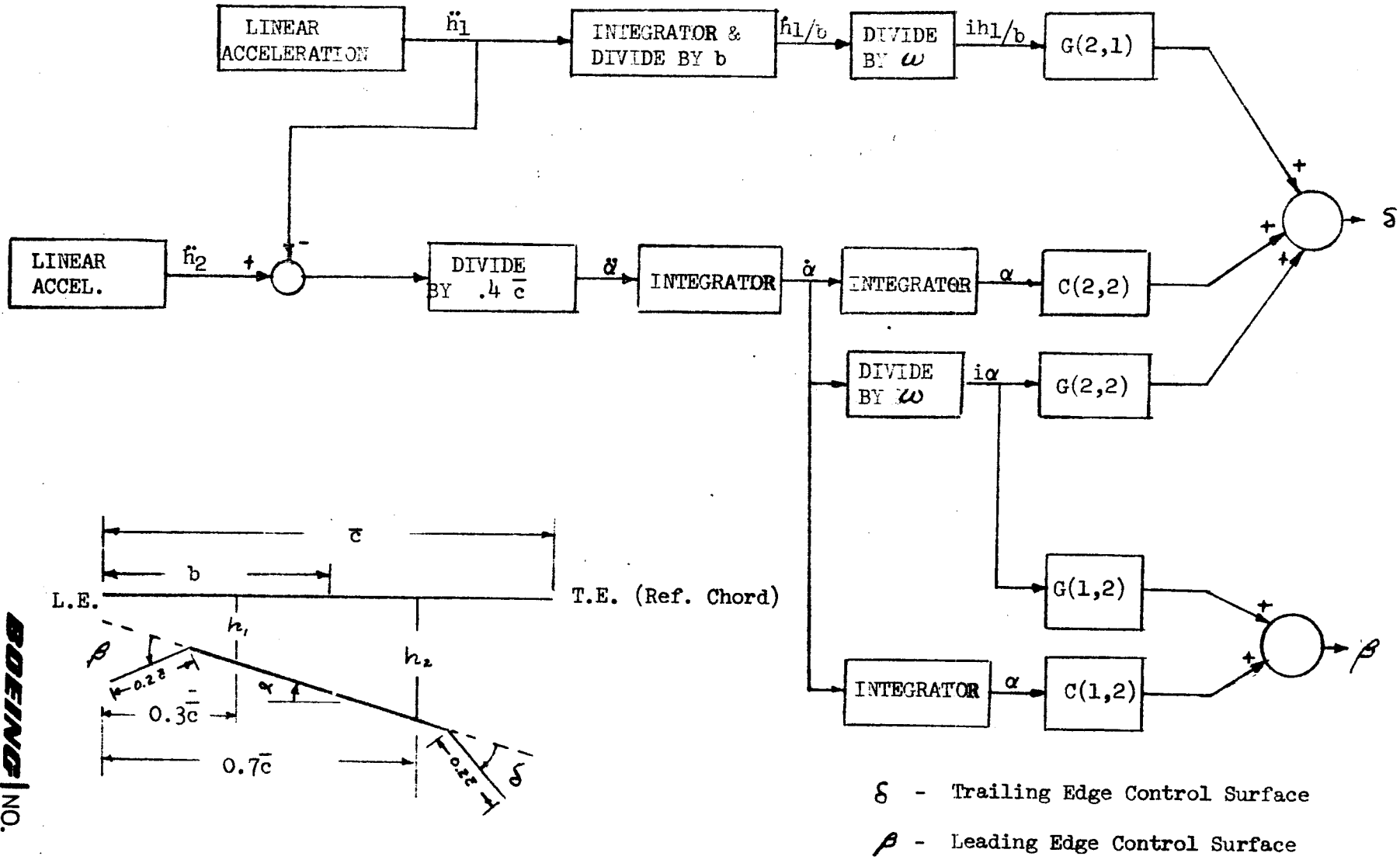

FLUTTER SAS BLOCK DIAGRAM

Figure 3

2.0 FLUTTER ANALYSIS

2.1 Full Scale SST Equations of Motion

Flutter analyses were conducted using the 969-300 SST configuration at Mach 0.9 and a gross weight of 395,000 pounds. The equations were modified to incorporate a 20 percent chord leading edge control surface. Figure 4 shows the location of the control surfaces, and Z (vertical translation) and θ (pitch angle) response stations for the wing. Vertical acceleration was sensed at chord (panel) stations that correspond to 30 and 70 percent chord.

The linear differential equations representing the 969-300 SST airplane configuration were written with forward speed and air density as explicit functions. This permitted varying the forward velocity as a function of altitude at constant Mach number to determine flutter speed. The math model includes two rigid body and ten structural modes. The aerodynamic theory used for the leading and trailing edge control surfaces was steady-state lifting surface with first-order lift growth approximations (Wagner functions) to represent unsteady aerodynamics.

2.2 Results

Both flutter SAS concepts employ a signal which has the same amplitude as displacement but is in phase with rate. This signal was generated for the stability study by using phase root locus to introduce a phase shift ($e^{j\theta}$) without changing the signal amplitude as a function of frequency. A block diagram of the system as arranged for stability analysis is shown in Figure 5.

Free airplane flutter is encountered when the third elastic mode crosses the imaginary axis at 422 KCAS. As speed is increased further the fourth elastic mode becomes unstable at 435 KCAS. The trailing edge control surface primarily stabilizes the fourth elastic mode whereas stability of the third mode is predominantly controlled with the leading/trailing edge surfaces. This conclusion is illustrated in Figure 6 by comparing the results for SAS No. 1 and No. 2 with outboard surfaces. Figure 7 shows the third and fourth mode damping ratio as a function of airspeed for the mid-span and inboard surfaces. Airspeed root locus plots for SAS No. 1 using a trailing edge surface and for SAS No. 2 using outboard, mid-span and inboard L/T edge surfaces are portrayed in Figures 8 through 11.

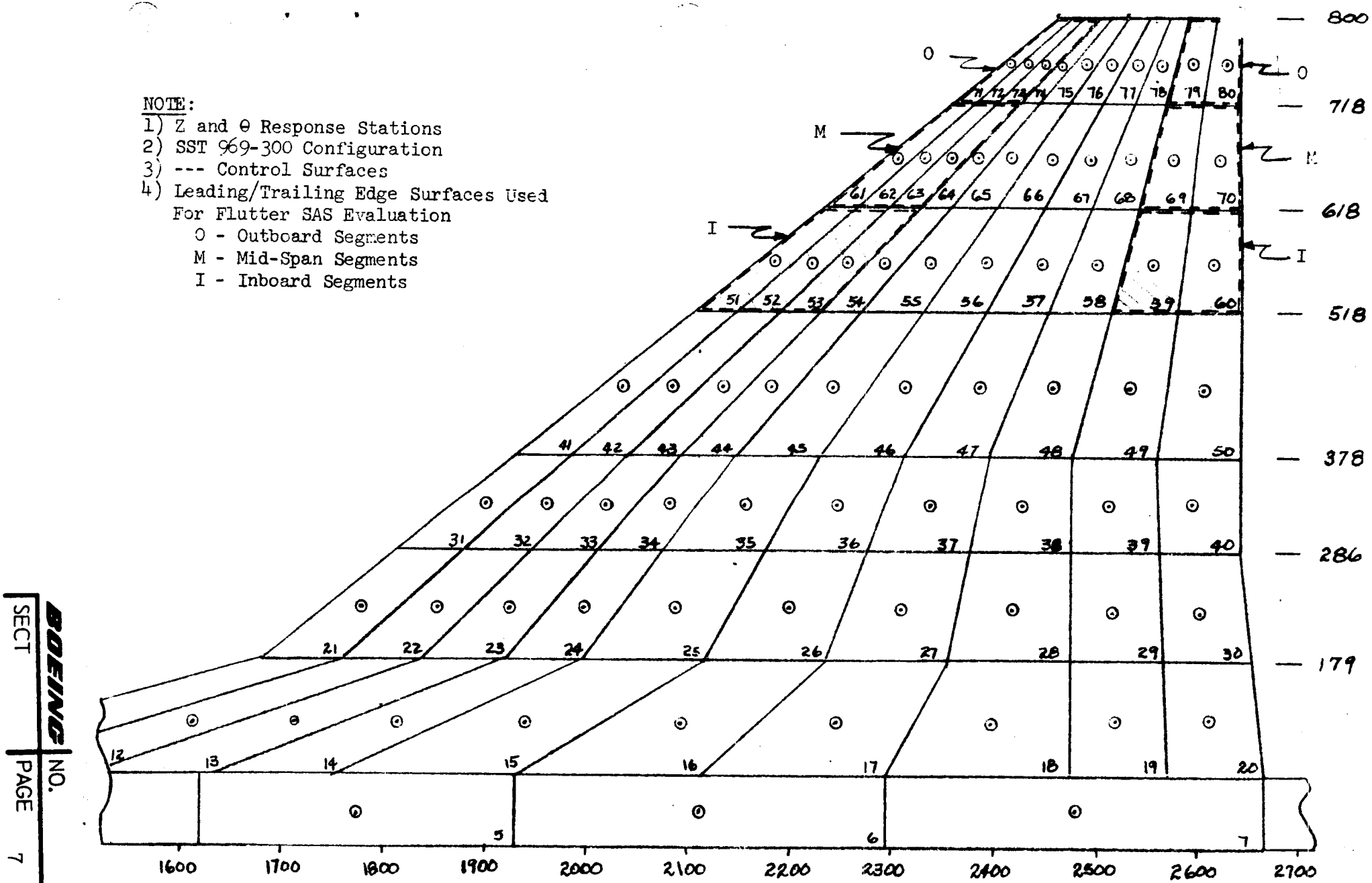

WING PANELING DIAGRAM

Figure 4

FLUTTER SAS DIAGRAM FOR STABILITY ANALYSIS
(Leading/Trailing Edge Control Surfaces)

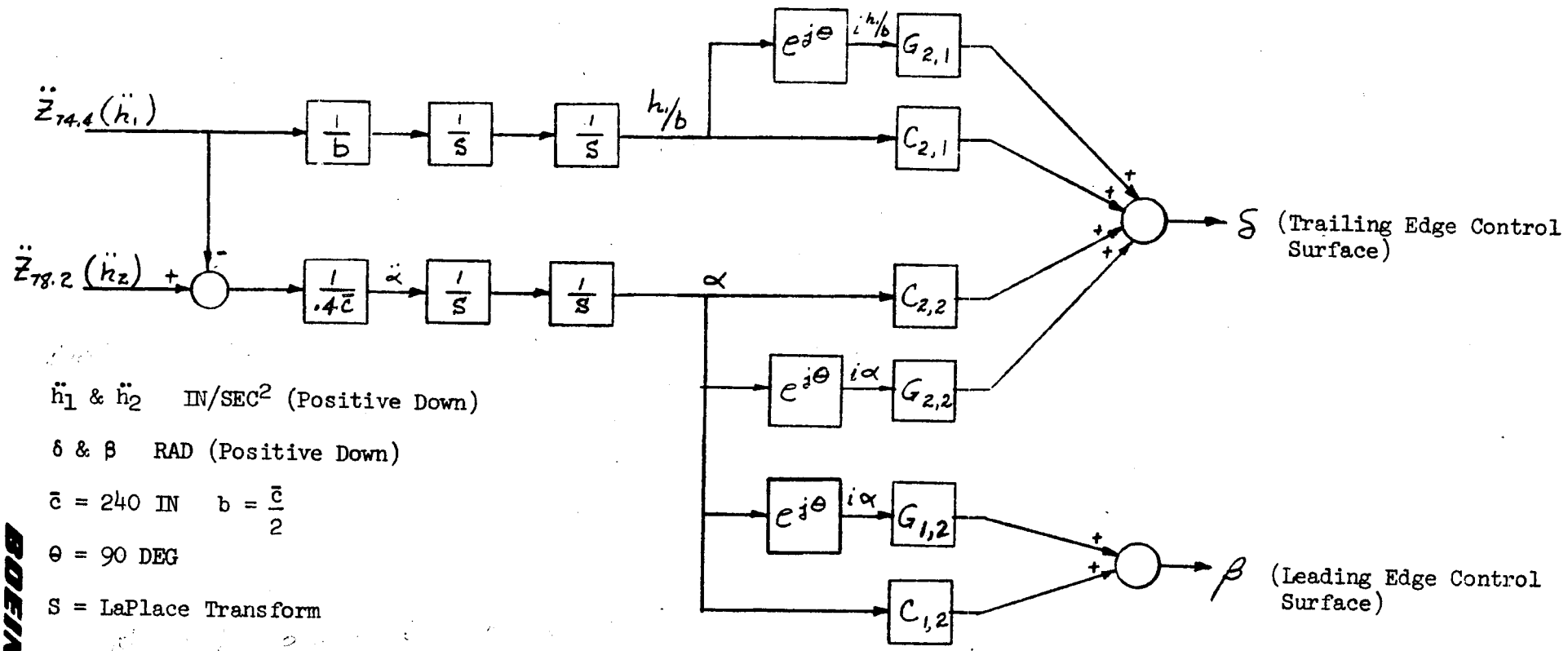

$\ddot{h}_1$ & $\ddot{h}_2$ IN/SEC^2 (Positive Down)

δ & β RAD (Positive Down)

$\bar{c}$ = 240 IN $\quad b = \frac{\bar{c}}{2}$

θ = 90 DEG

S = LaPlace Transform

BOEING SECT NO. PAGE 8

$$\begin{Bmatrix}\beta\\ \delta\end{Bmatrix} = \underbrace{\begin{bmatrix}0 & 0\\ -0.35 & -1.9\end{bmatrix}}_{C}\begin{Bmatrix}h_1/b\\ \alpha\end{Bmatrix} + e^{j\theta}\underbrace{\begin{bmatrix}0 & 0\\ 0.35 & 0.1\end{bmatrix}}_{G}\begin{Bmatrix}h_1/b\\ \alpha\end{Bmatrix}$$

FLUTTER SAS NO. 1
TRAILING EDGE CONTROL ONLY

$$\begin{Bmatrix}\beta\\ \delta\end{Bmatrix} = \begin{bmatrix}0 & 5.6\\ 0 & -1.4\end{bmatrix}\begin{Bmatrix}h_1/b\\ \alpha\end{Bmatrix} + e^{j\theta}\begin{bmatrix}0 & 1.5\\ 0.6 & 0.2\end{bmatrix}\begin{Bmatrix}h_1/b\\ \alpha\end{Bmatrix}$$

FLUTTER SAS NO. 2
TRAILING AND LEADING EDGE CONTROL

Figure 5

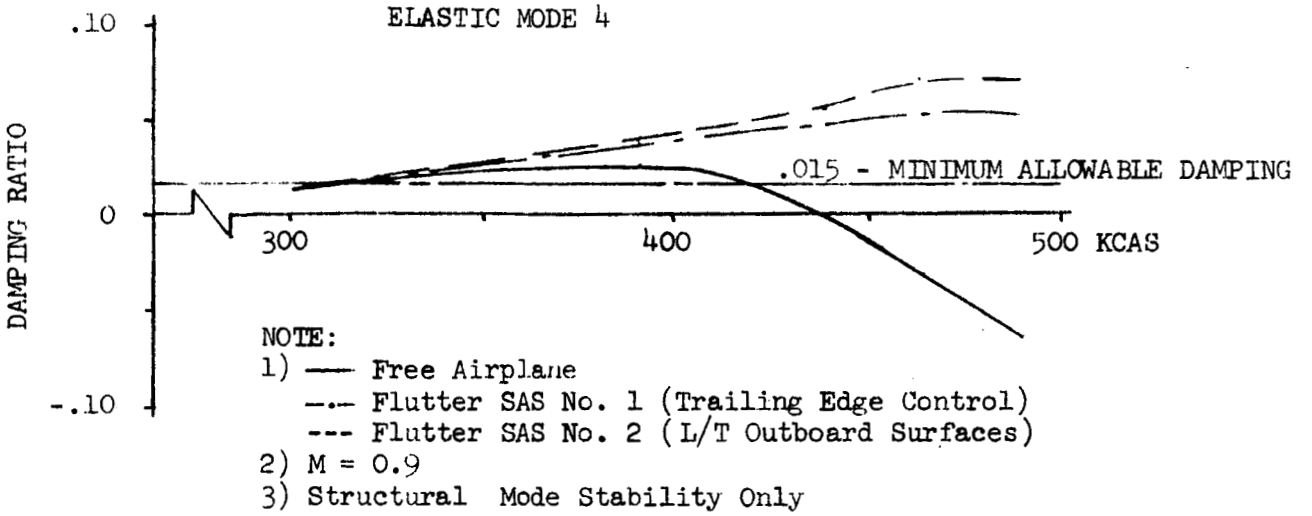

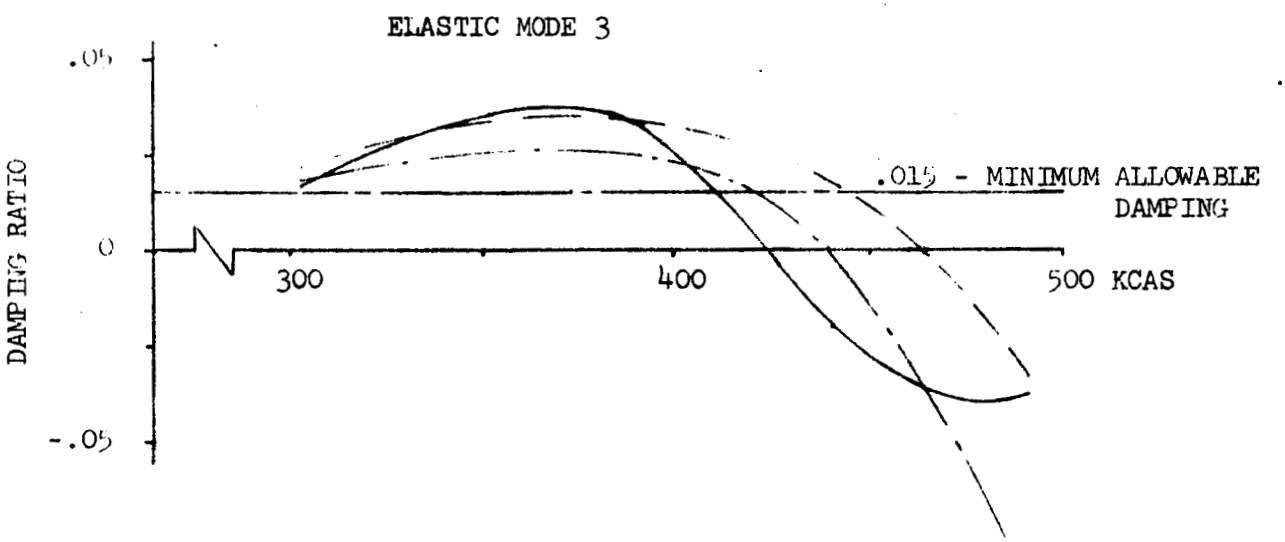

EFFECT OF SAS ON FLUTTER SPEED

Figure 6

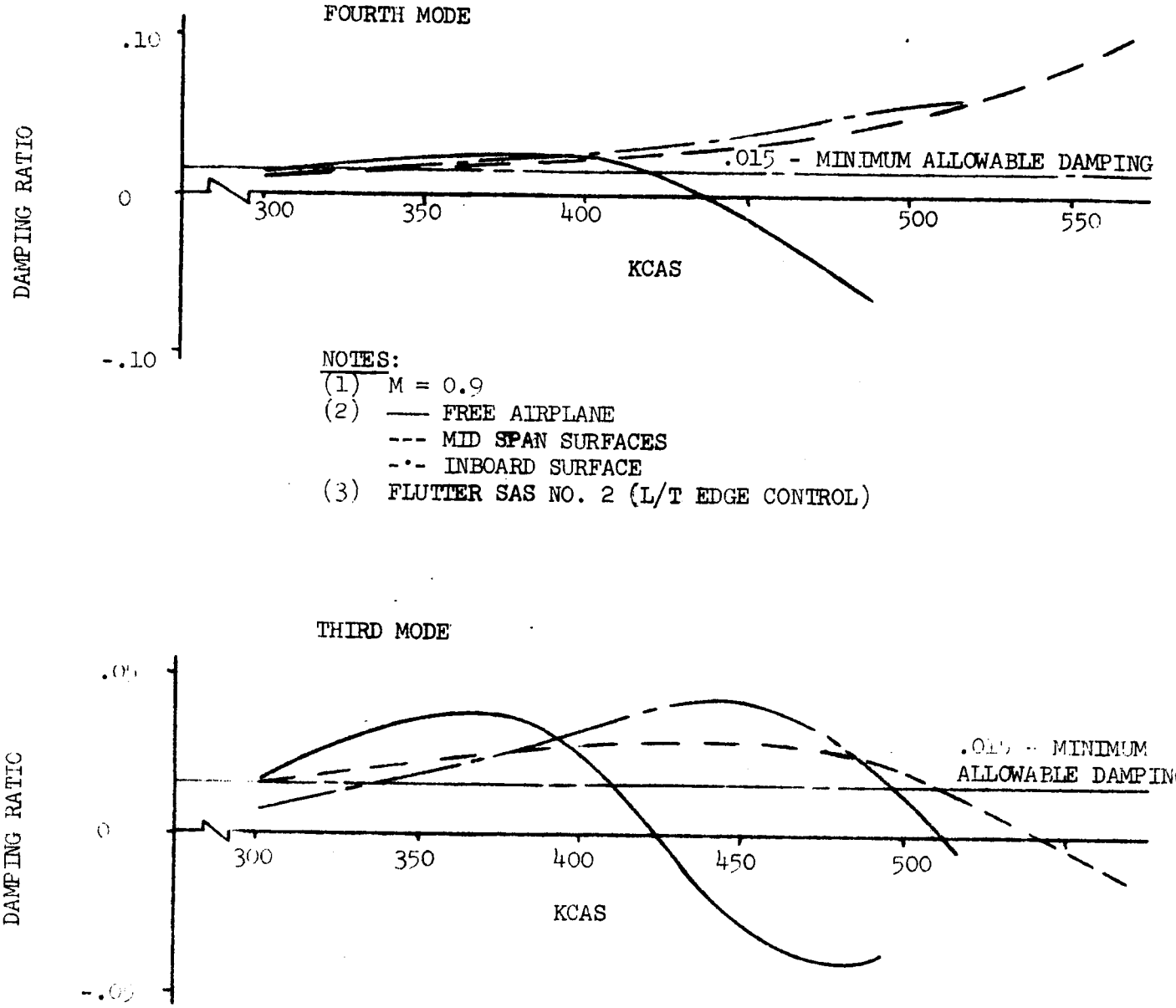

EFFECT OF SAS ON FLUTTER SPEED

Figure 7

NOTE:

1) M = 0.9
2) —— Free Airplane
3) --- With Flutter SAS No. 1
4) Flutter Speed (3rd Mode)
   FREE AIRPLANE: 422 KCAS
   WITH SAS: 440 KCAS

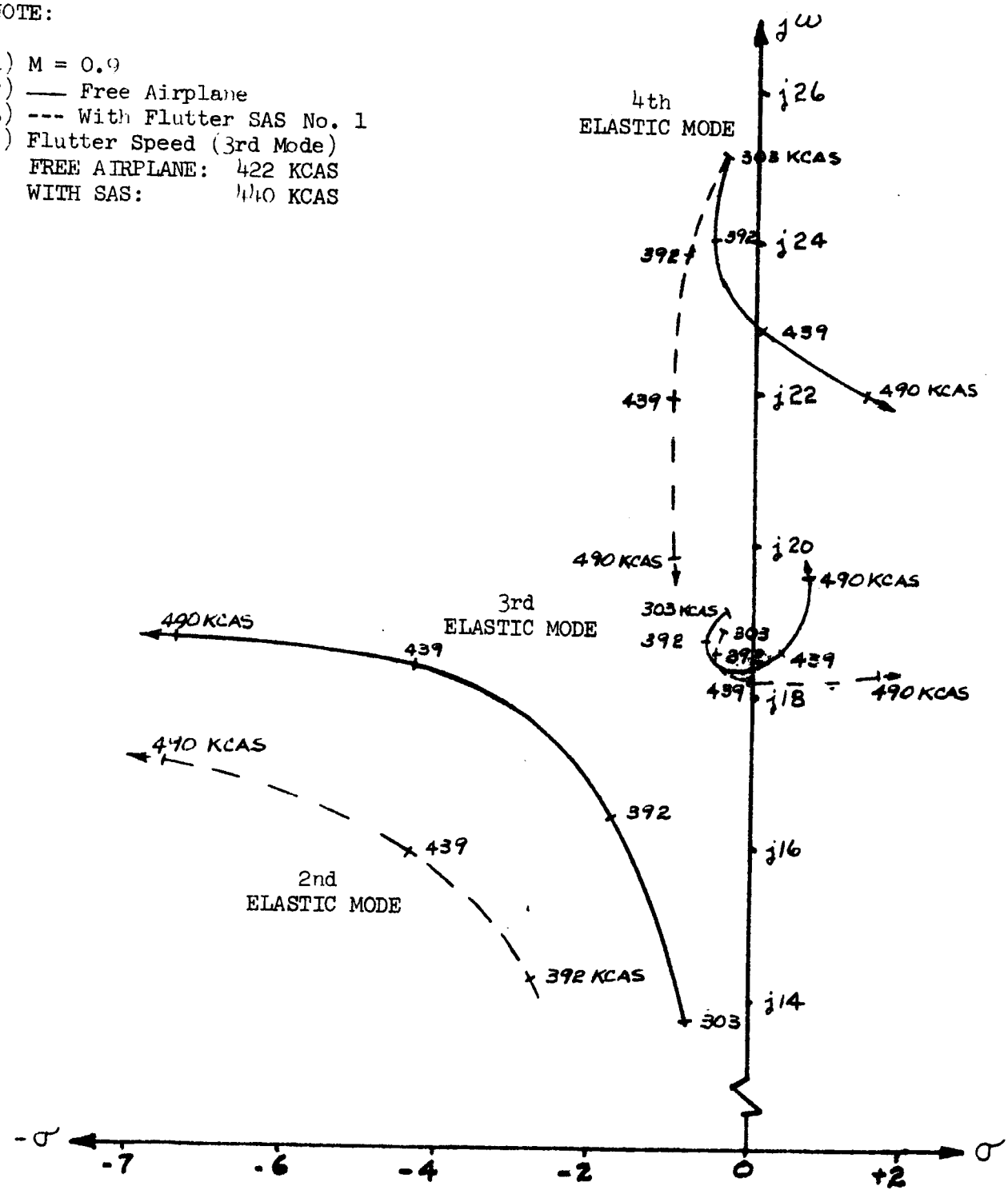

FLUTTER SAS ROOT LOCUS
WITH TRAILING EDGE CONTROL SURFACE

Figure 8

NOTES:

1) M = 0.9
2) ___ Free Airplane
3) --- With Flutter SAS No. 2
4) Flutter Speed (3rd Mode)
   Free Airplane: 422 KCAS
   With SAS: 464 KCAS

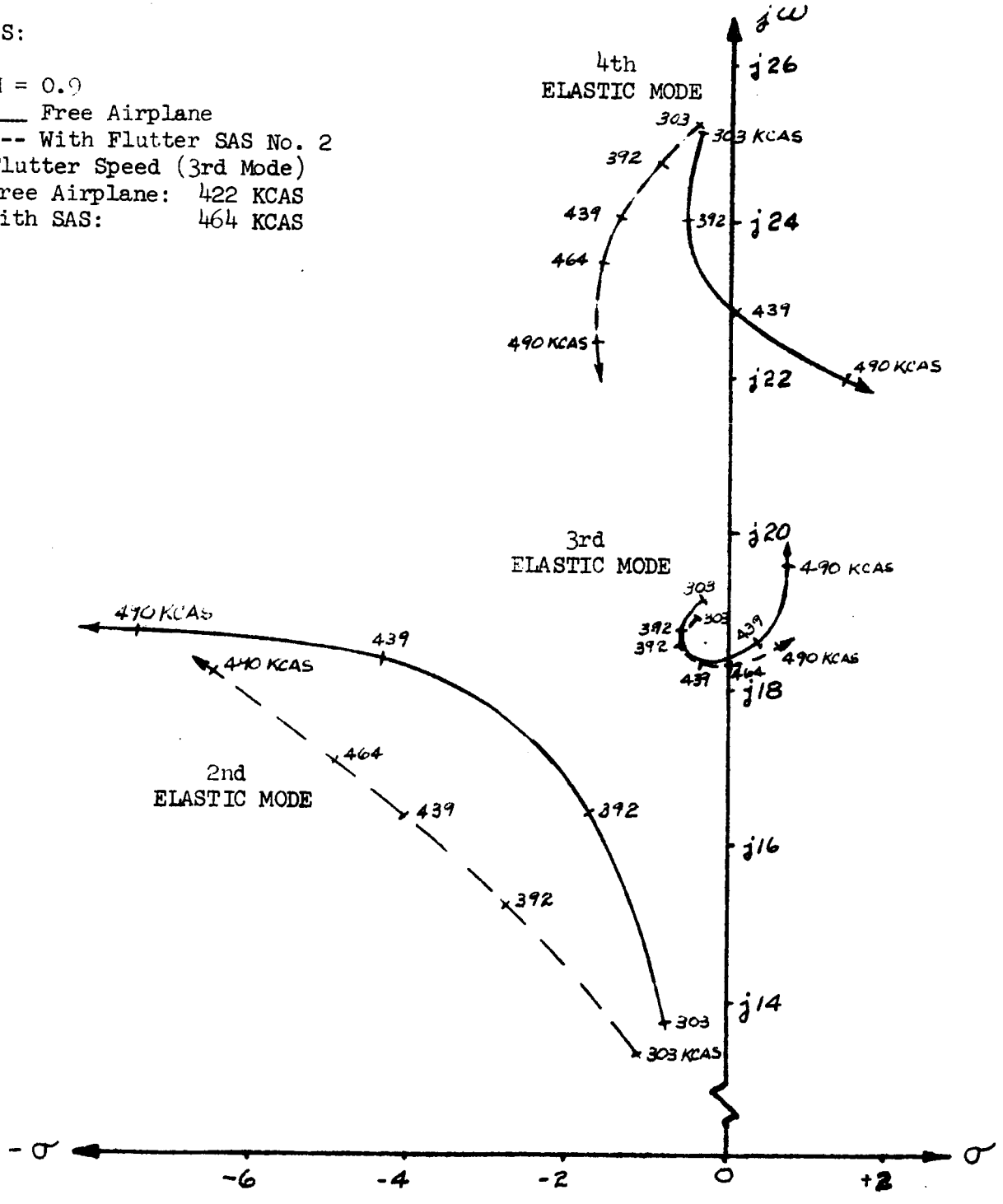

FLUTTER SAS ROOT LOCUS
WITH OUTBOARD L/T EDGE CONTROL SURFACES

Figure 9

NOTES:
1) M = 0.9
2) —— FREE AIRPLANE
3) --- WITH FLUTTER SAS NO. 2
4) FLUTTER SPEED (3RD MODE)
   FREE AIRPLANE: 422 KCAS
   WITH SAS: 540 KCAS

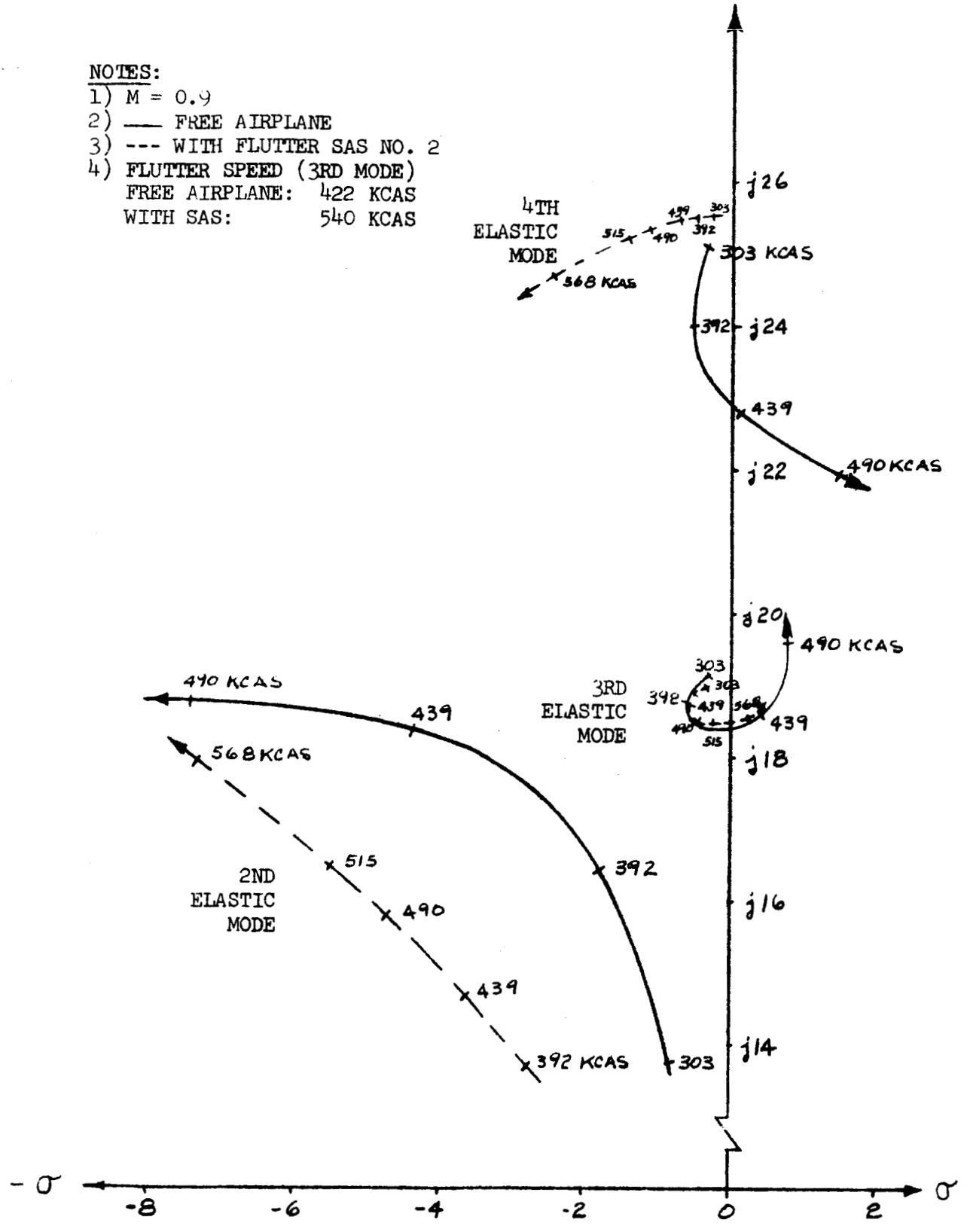

FLUTTER SAS ROOT LOCUS
WITH MID-SPAN L/T EDGE SURFACES

FIGURE 10

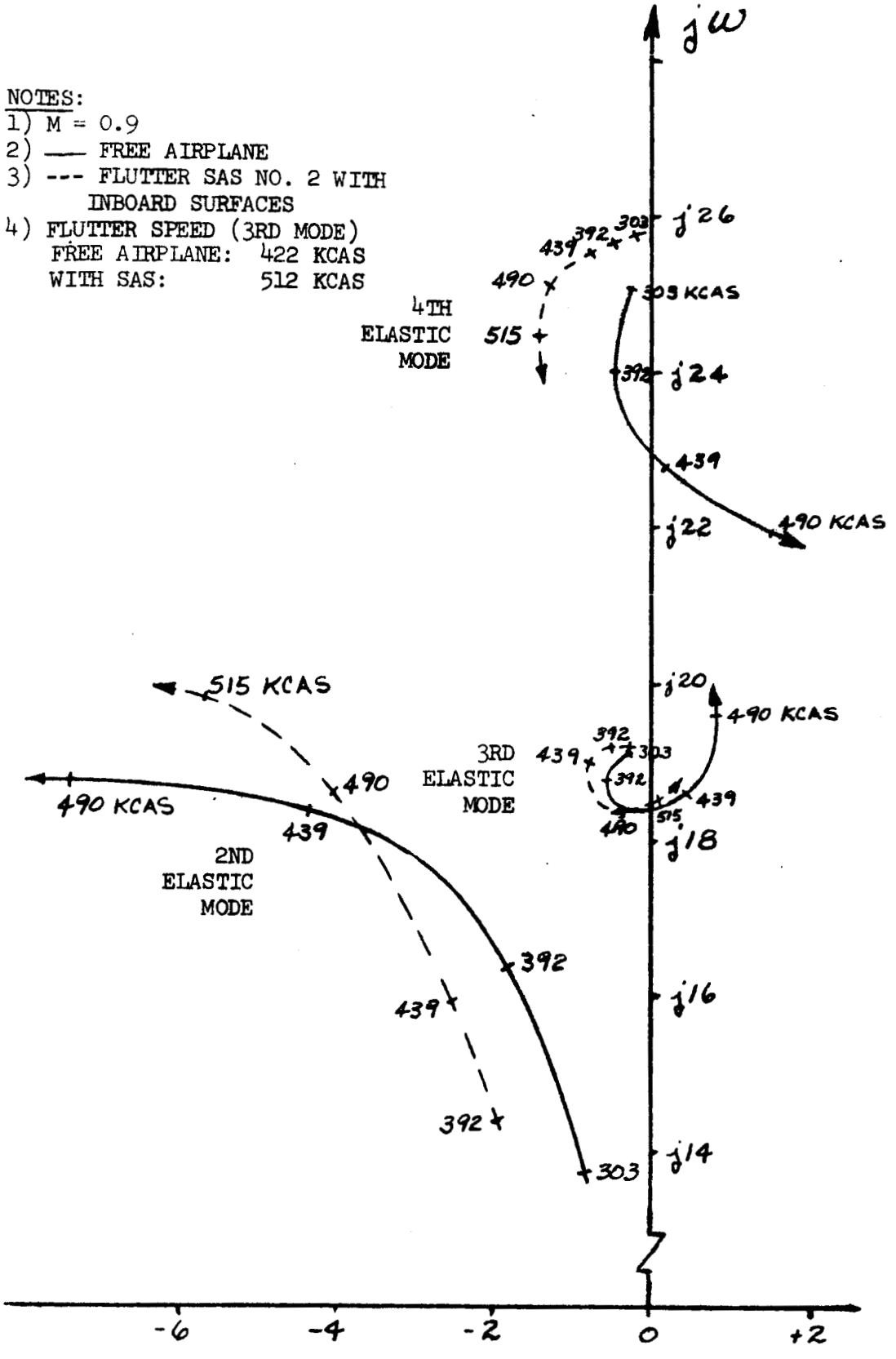

FLUTTER SAS ROOT LOCUS
WITH INBOARD L/T EDGE SURFACES

Figure 11

3.0 FLUTTER SAS MECHANIZATION

To mechanize these flutter SAS concepts it is necessary to measure the feedback signal frequency (or period) or to generate 90 degrees phase lead. An analog computer simulation was developed to assess the feasibility of measuring frequency using analog components. The "frequency" measurement was based on the simple harmonic motion relationship: $\omega^2 = |\text{acceleration}|/|\text{displacement}|$. Sections 3.1 and 3.2 describe the mechanization and performance of this technique.

A second analog simulation was utilized to evaluate a technique that measures the signal "period". This method eliminates some division and square root circuits associated with the frequency method. Section 3.3 describes the mechanization and performance of this system.

3.1 Description of Computer Circuit for Measuring Frequency

An analog computer diagram for one channel of the SAS is shown in Figure 12. The numerator and denominator terms which form the radian frequency (ω) are passed through approximate derivative circuits to eliminate any d.c. bias in either signal. The voltage signals from the derivative circuits are then rectified to accommodate the electronic multiplier division circuit producing ω_1^2.

Threshold logic was mechanized using a relay comparator to alleviate the noise amplification produced by the division circuit when the numerator and denominator voltages are small. When the voltage representing the denominator, $|Z_2|$, is above the threshold value the frequency is formed by the equation $\omega_1^2 = |\ddot{Z}_2 / Z_2|$. When this voltage is less than the threshold, the value of ω_1^2 before the relay switches is stored. This mechanization also eliminates division by zero when the oscillatory transient solution of the plant equations decays to zero, leaving only the steady state solution (as for a step plant disturbance).

While the relay comparator is switching, the numerator and denominator voltages are both momentarily zero which causes the amplifiers in the division circuit to saturate. This produces the spikes on the time history for ω_1^2 shown in Figure 13 and, without filtering, these spikes appear in the square root as well. Several first order filters were tried to alleviate this difficulty. The time histories shown in Figure 13 were recorded with the filter $G(S) = \frac{10}{S+10}$.

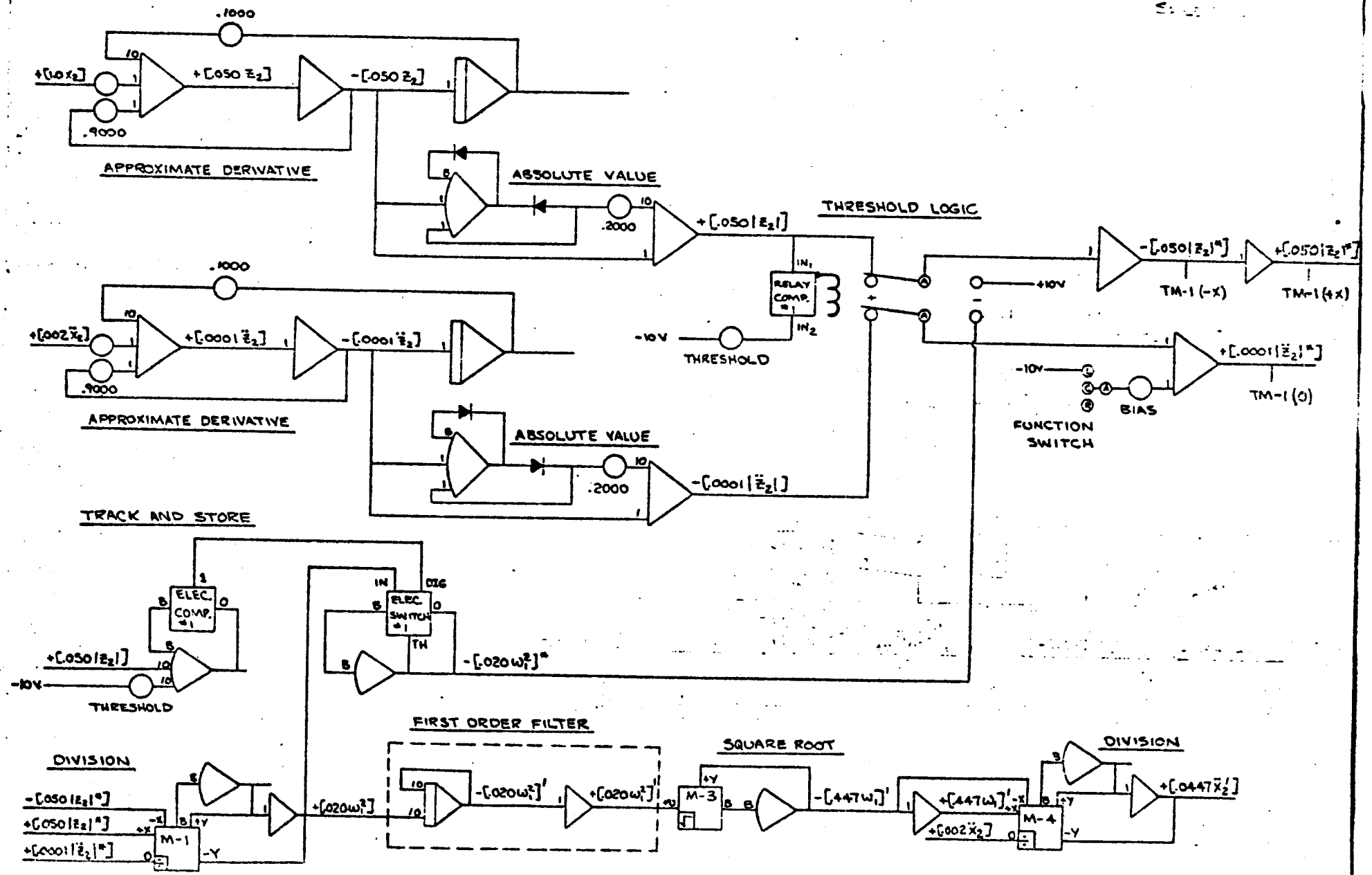

FIGURE 12. ANALOG CIRCUIT DIAGRAM (SINGE CHANNEL)

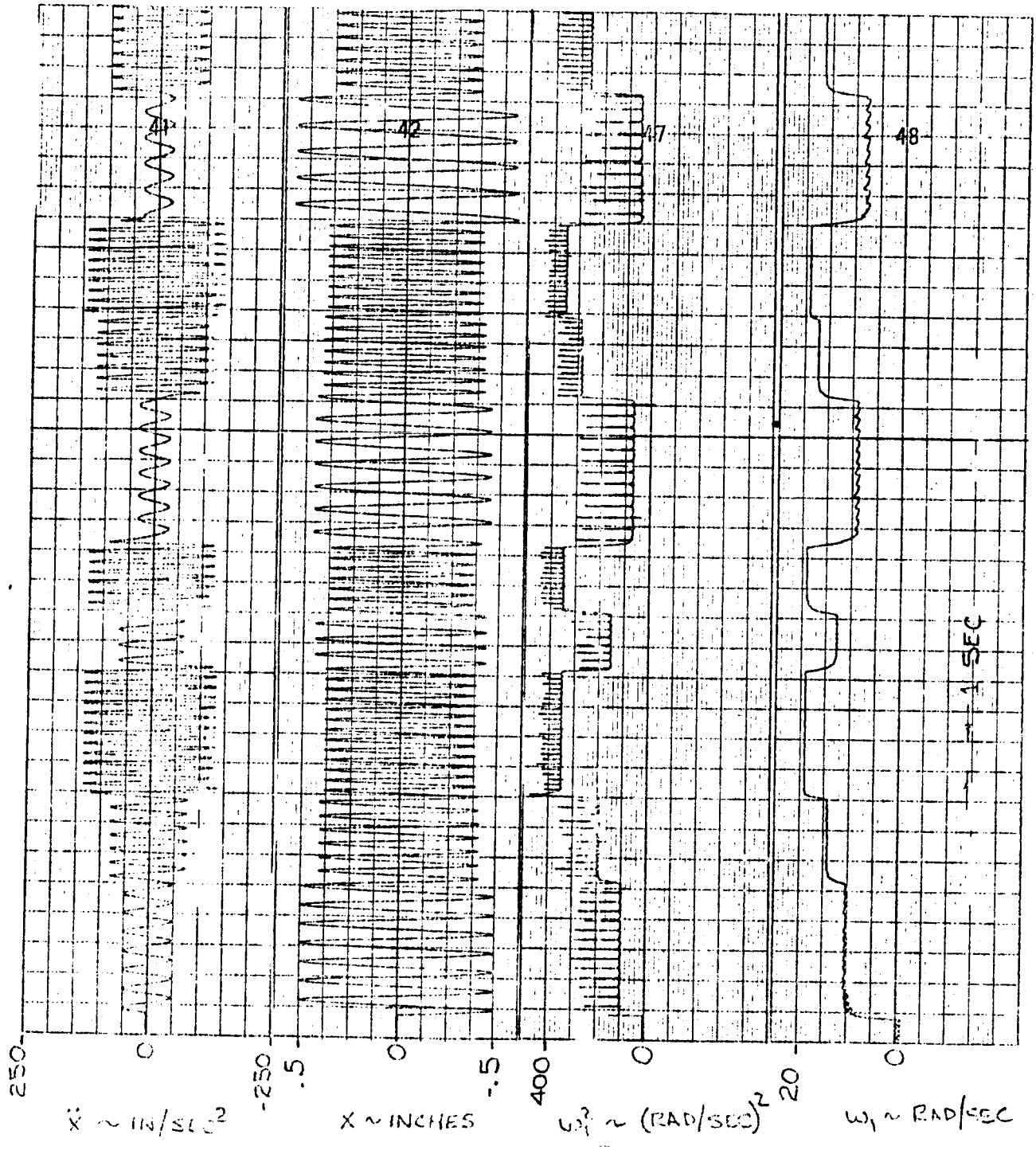

FIGURE 13

FREQUENCY MEASURING CIRCUIT PERFORMANCE

The analog components required to mechanize this single channel on the TR-48 computer are tabulated below:

20 Summing Amplifiers
3 Integrating Amplifiers
1 Relay Comparator
1 Electronic Comparator and Switch
3 Electronic Multipliers
11 Potentiometers

3.2 Frequency Measuring Circuit Performance

The capability of the mechanization to measure instantaneous frequency for simple harmonic motion is illustrated in Figure 14. This figure shows the acceleration, displacement, radian frequency squared, and the radian frequency for step changes in frequency.

The ratio which forms the radian "frequency" is not constant, in general, for a multi-degree-of-freedom plant containing more than one oscillatory mode. This is due to each degree-of-freedom consisting of a weighted sum of all the oscillatory modes. Figure 14 shows this for a coupled two degree-of-freedom plant with two lightly damped modes. This figure shows the two displacements and the radian "frequency" formed by the ratio $|\ddot{x}_3 - \ddot{x}_2|/|x_3 - x_2|$.

3.3 Period Measuring Mechanization and Performance

Figure 15 illustrates the performance of the "period" measuring mechanization for simple harmonic motion. The figure shows the system response for input oscillations of 5 and 50 Hz. This method measures the "period" by detecting zero-crossings. The system updates after each zero-crossing and holds this value until the next crossing. Therefore, the measured "period" is not instantaneous. An analog circuit diagram and signal sketches for one channel of the SAS is presented in Figure 16. This approach to measuring the period forces a trade-off between accuracy at low frequency and speed of response since a first-order lag is used as an approximate integrator. Its associated time constant determines how fast the voltage on the integrator changes.

The data indicates that the steady-state error in the frequency range of interest (5 to 25 Hz) is less than 3 percent. The transient response for a step change in frequency has a nominal rise time of approximately 0.25 seconds. This value increases approximately 50 percent when the step change occurs at the maximum integrator voltage.

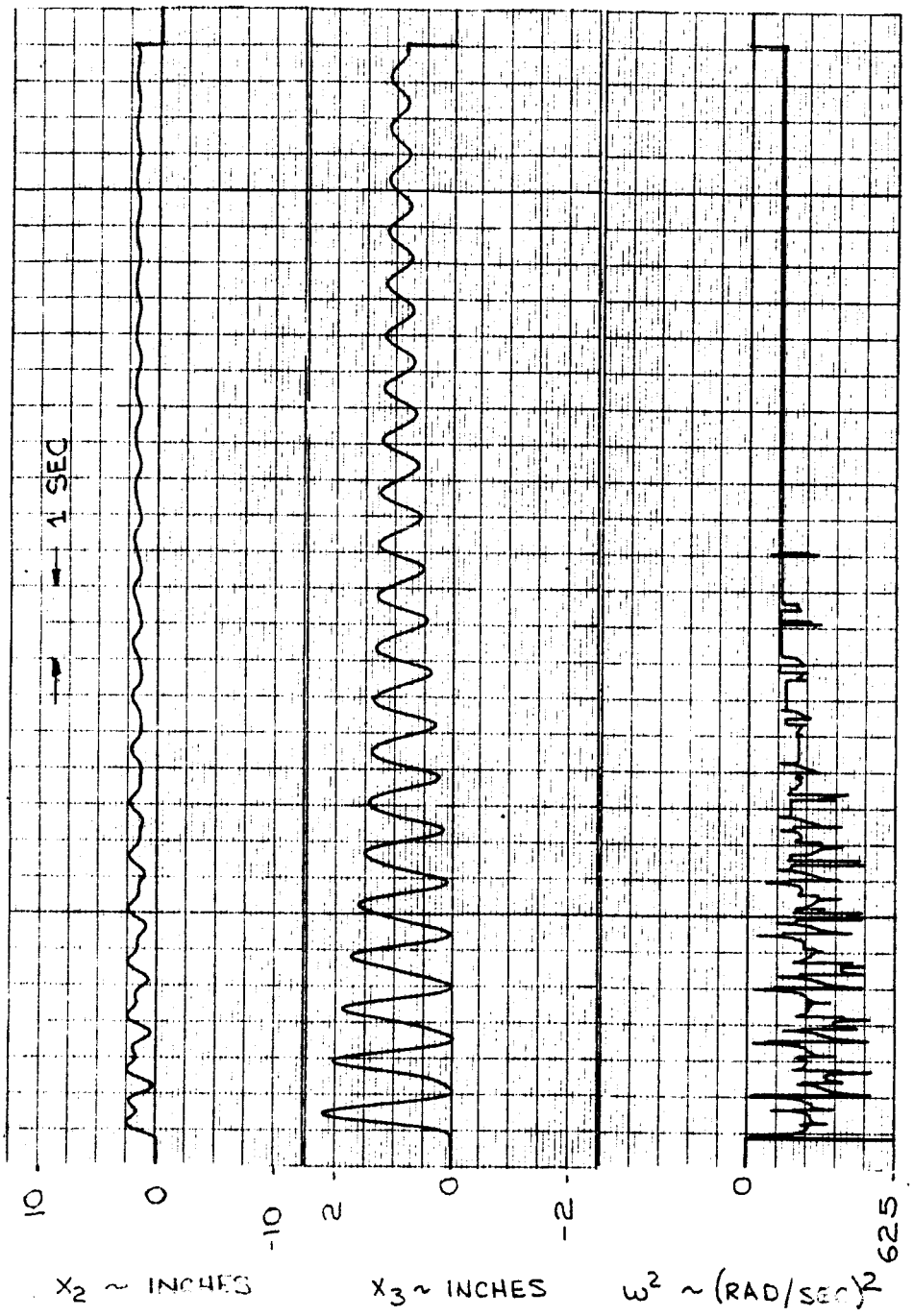

FREQUENCY MEASURING CIRCUIT PERFORMANCE
FOR TWO DOF PLANT

FIGURE 14

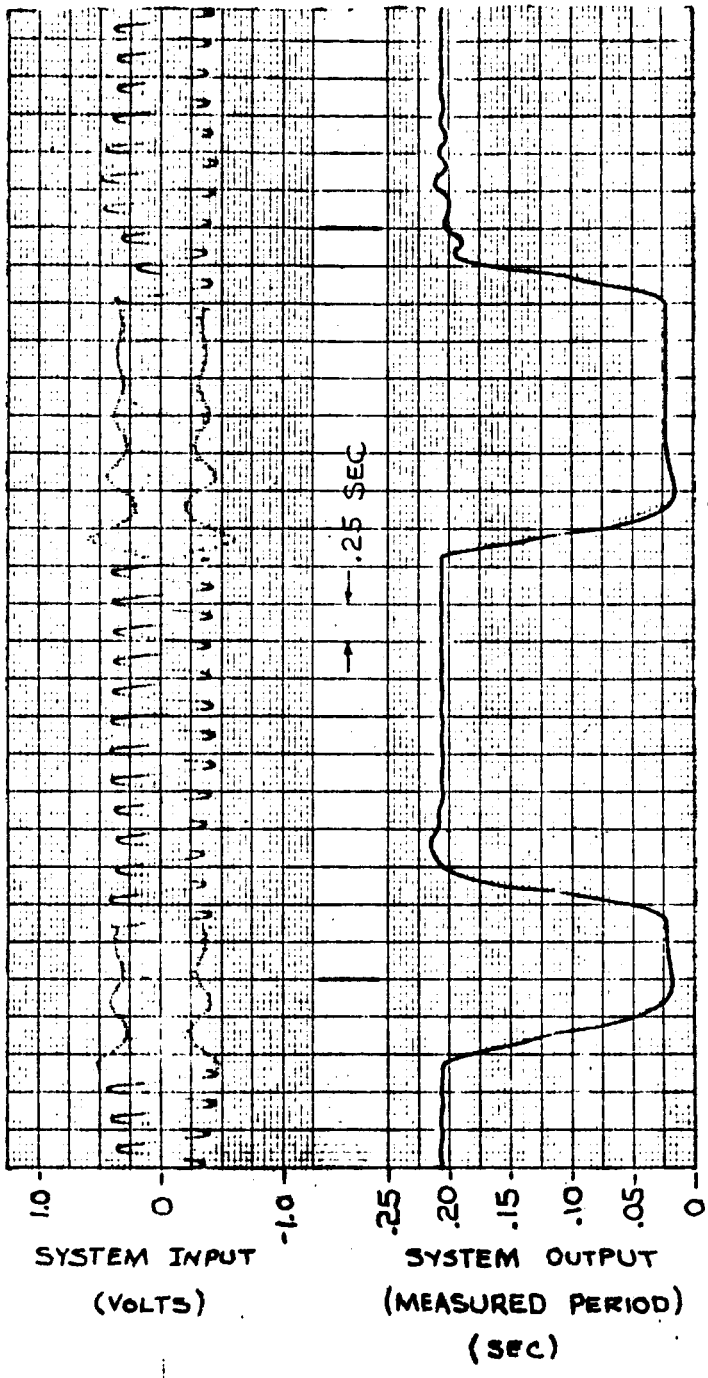

PERIOD MEASURING CIRCUIT PERFORMANCE

FIGURE 15

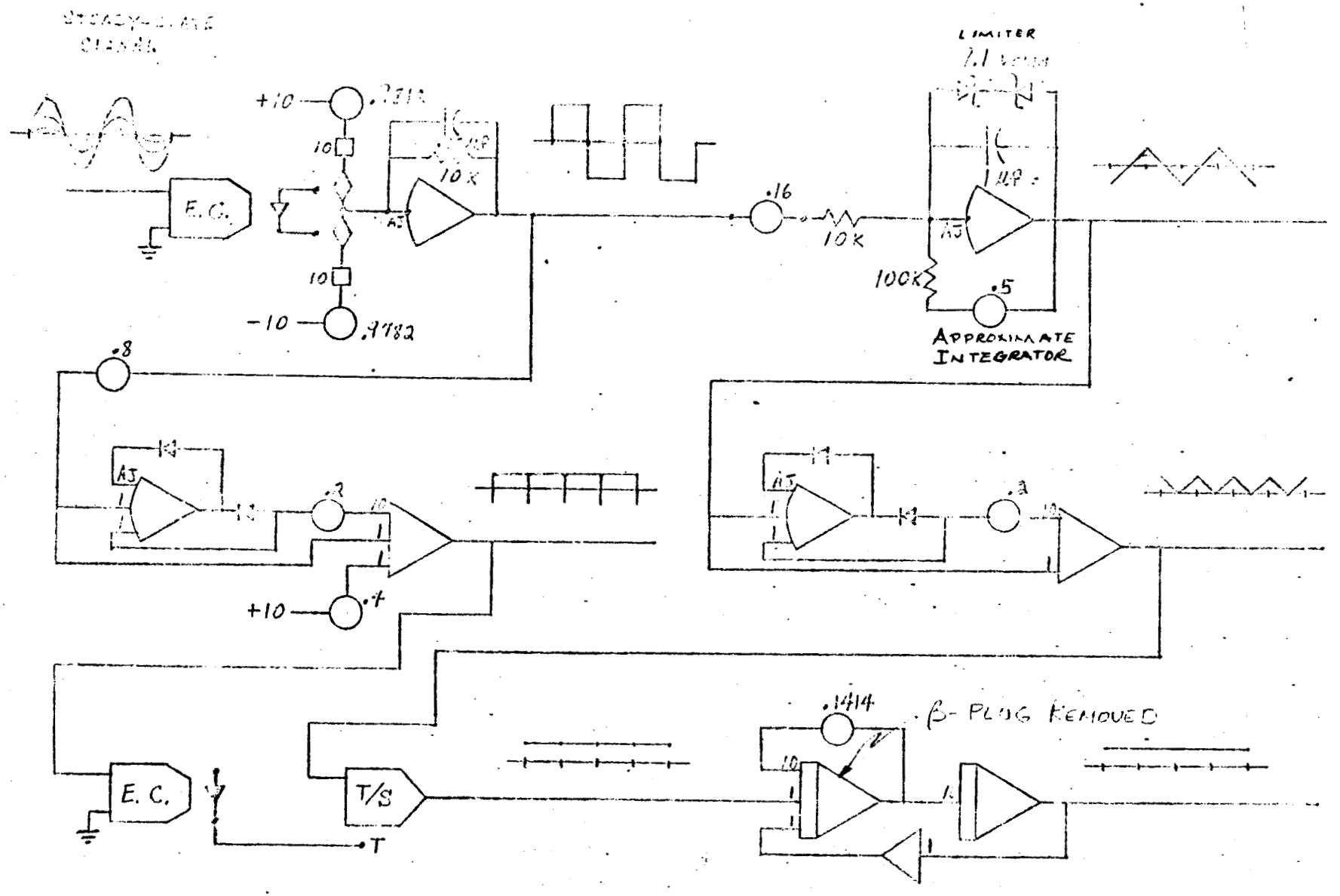

NOTE: 1) SCALE FACTOR : .025 SEC/VOLT

FIGURE 16. PERIOD MEASURING SYSTEM

ANALOG DIAGRAM AND SIGNAL SYMBOLS